Electrically induced insulator to metal transition in epitaxial SmNiO3 thin films

Nikhil Shukla, Toyanath Joshi, Sandeepan Dasgupta, Pavel Borisov, David Lederman, and Suman Datta

Citation: Applied Physics Letters **105**, 012108 (2014); doi: 10.1063/1.4890329
View online: http://dx.doi.org/10.1063/1.4890329
View Table of Contents: http://scitation.aip.org/content/aip/journal/apl/105/1?ver=pdfcov
Published by the AIP Publishing

APPLIED PHYSICS LETTERS **105**, 012108 (2014)

Electrically induced insulator to metal transition in epitaxial $SmNiO_3$ thin films

Nikhil Shukla,[1,a)] Toyanath Joshi,[2] Sandeepan Dasgupta,[1] Pavel Borisov,[2] David Lederman,[2] and Suman Datta[1]

[1]*Department of Electrical Engineering, The Pennsylvania State University, University Park, Pennsylvania 16802, USA*

[2]*Department of Physics and Astronomy, West Virginia University, Morgantown, West Virginia 26506-6315, USA*

(Received 3 June 2014; accepted 3 July 2014; published online 11 July 2014)

We report on the electrically induced insulator to metal transition (IMT) in $SmNiO_3$ thin films grown on (001) $LaAlO_3$ by pulsed laser deposition. The behavior of the resistivity as a function of temperature suggests that the primary transport mechanism in the $SmNiO_3$ insulating state is dominated by Efros-Shklovskii variable range hopping (ES-VRH). Additionally, the magnetic transition in the insulating state of $SmNiO_3$ modifies the characteristics of the ES-VRH transport. Systematic DC and pulsed current-voltage measurements indicate that current-induced joule heating is the fundamental mechanism driving the electrically induced IMT in $SmNiO_3$. These transport properties are explained in context of the IMT in $SmNiO_3$ being related to the strong electron-lattice coupling. © *2014 AIP Publishing LLC*. [http://dx.doi.org/10.1063/1.4890329]

Perovskite rare-earth nickelates ($RNiO_3$) exhibit a prototypical thermally driven insulator to metal transition (IMT) (except for bulk $LaNiO_3$, which is a metal at all temperatures).[1] This along with competing interactions involving the lattice, orbital, spin, and charge degrees of freedom, which may be responsible for the IMT, make this material system the object of intense fundamental and applied research interest.[2–11] The IMT in the $RNiO_3$ system usually consists of a transition from a low temperature insulating phase to a high temperature metallic phase with a bad-metal character.[12] The phase diagram of $RNiO_3$ compounds is controlled by the radius of the R^{3+} atom, which in turn determines the tilting angle of $(NiO_6)^{3-}$ octahedra.[13,14] The IMT temperature (T_{IMT}) decreases as the ionic radius of the R^{3+} atom increases.[15] Nickelates also exhibit magnetic ordering.[16,17] In the case of $PrNiO_3$ and $NdNiO_3$, the Neel temperature (T_N) of antiferromagnetic ordering coincides with the IMT temperature (T_{IMT}). For Sm and smaller rare-earth metal ions, $T_N < T_{IMT}$.

$SmNiO_3$ exhibits an IMT above room temperature ($T_{IMT} \sim 400$ K) transitioning from a low temperature insulating phase to a high temperature metallic phase. In this Letter, the electrically driven IMT in two terminal $SmNiO_3$ thin film devices using DC and pulse mode current-voltage (I-V) measurements is described. The ability to induce an IMT via an electric field is relevant to realizing electronic applications.[18,19] The mechanism of the electrically driven phase transition was investigated by applying the driving stimulus (I,V) using different time scales (200 ns–10 s) as a function of temperature.

$SmNiO_3$ thin films with a thickness of 16 nm were epitaxially grown on polished $LaAlO_3$ (001) substrates (MTI Corp.) by a pulsed laser deposition (PLD) system (Neocera) using a 248 nm KrF excimer laser (Coherent). A polycrystalline $SmNiO_3$ target of 99.99% purity (Shanghai Daheng Optics) was used. During growth, the substrate's nominal temperature was at 1023 K in 33.3 Pa dynamic pressure of flowing O_2 with a laser pulse repetition rate of 5 Hz and a laser fluence of approximately 2 J/cm^2. After growth, the films were cooled at 20 K/min under the same O_2 pressure. The growth rate was calibrated using x-ray reflectometry (XRR). The structural quality of the substrate and the film was verified *in-situ* by reflection high-energy electron diffraction (RHEED) and *ex-situ* by x-ray diffraction (XRD) on a four circle diffractometer. Two terminal devices with dimensions $L = 2\,\mu$m; $W = 4\,\mu$m were fabricated using standard photolithographic techniques. The width of the device was defined by the contact pad. Ti/Au (40 nm/50 nm) was used for the contact pads resulting in ohmic contacts.

Figure 1(a) shows RHEED images taken from an as-grown thin film. The streaky nature and in-plane symmetry of the patterns revealed that the film surface was single-crystalline. Based on the RHEED results and the XRD Φ-scans of $SmNiO_3$ (101) and $LaAlO_3$ (111) pseudo-cubic peaks (Fig. 1(d)), we determined that the in-plane orientation of the pseudo-cubic unit cell vectors in $SmNiO_3$ coincide with the pseudo-cubic lattice vectors of the $LaAlO_3$ substrate. The same out-of-plane pseudo-cubic orientation, $SmNiO_3$ [001] || $LaAlO_3$ [001], was confirmed by XRD patterns (Fig. 1(b)), yielding an out-of-plane pseudo-cubic lattice constant $a = 3.81$ Å for $SmNiO_3$ resulting in a -0.6% mismatch with the substrate. The corresponding XRD rocking curve full width at half maximum (FWHM) value was $0.61°$ for the (002) $SmNiO_3$ peak (Fig. 1(c)).

The temperature dependent resistivity $\rho(T)$ of the $SmNiO_3$ film is shown in Fig. 2(a). The large change in resistivity, of over three orders of magnitude between 100 K and 400 K, further corroborates the good film quality. This epitaxially strained $SmNiO_3$ film undergoes an IMT at 393 K as indicated by the minimum in the $|d\rho/dT|$ (Fig. 2(a)).

To understand the nature of transport in the insulating phase of $SmNiO_3$, we plot $\ln(\rho)$ versus T^{α}, where $\alpha = -1$ corresponds to Arhenius-type thermally activated conduction

[a)]Electronic mail: nss152@psu.edu

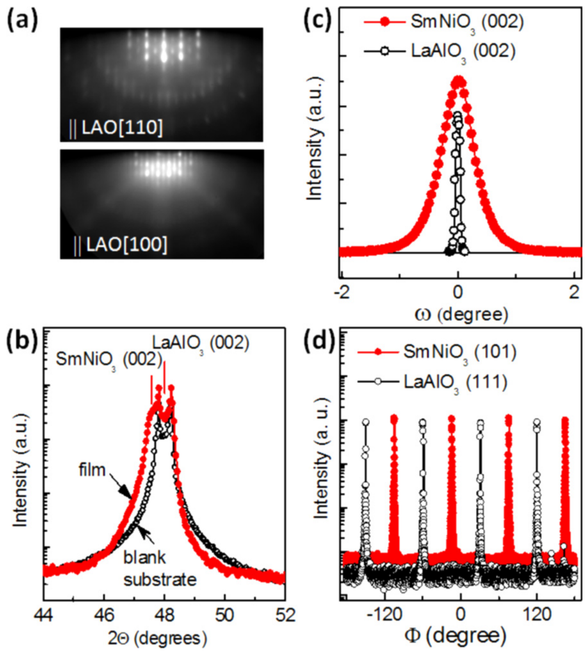

FIG. 1. (a) RHEED patterns for the $SmNiO_3$ thin film along the [110] and [100] azimuth of the $LaAlO_3$ (001) substrate, respectively. (b) XRD pattern from a $SmNiO_3$ film (solid circles) and from a blank $LaAlO_3$ (001) substrate (open circles, please note detector saturation at the $LaAlO_3$ (002) peak), respectively. (c) Rocking curves of the (002) peaks of the $SmNiO_3$ film (solid circles) and the $LaAlO_3$ substrate (open circles), respectively. (d) Φ scan of (101) and (111) peaks for the $SmNiO_3$ film (solid circles) and $LaAlO_3$ substrate (open circles), respectively.

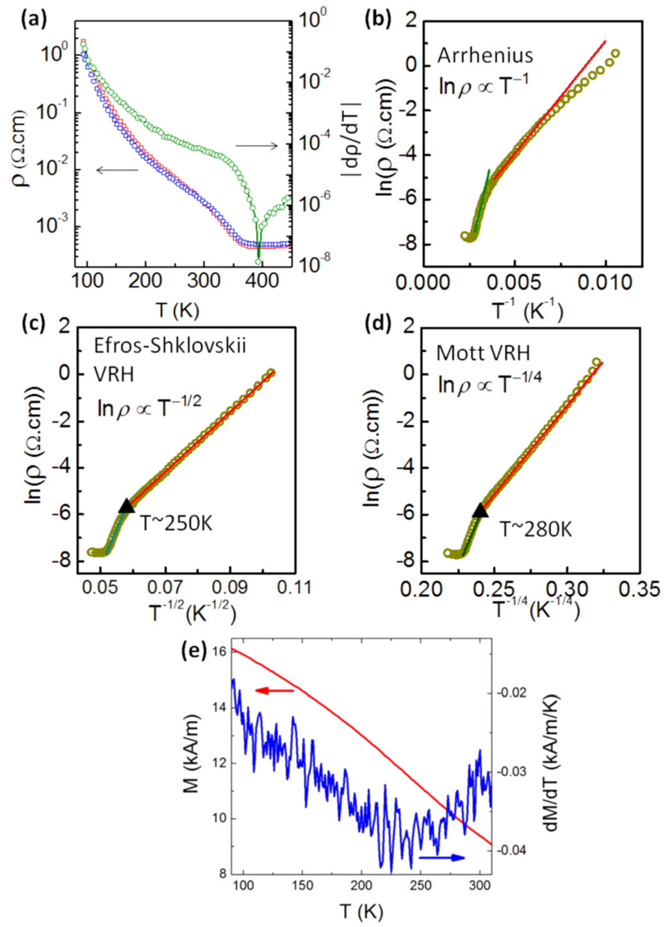

FIG. 2. (a) Variation of resistivity (ρ) as the function of temperature (T). The minimum value of $|d\rho/dT|$ at 393 K indicates that the IMT in the $SmNiO_3$ film occurs at this temperature. (b) ρ versus T characteristics plotted as $\ln(\rho)$ versus T^{-1} for the $SmNiO_3$ film to verify Arrhenius-type hopping transport mechanism (c) ρ versus T characteristics plotted as $\ln(\rho)$ versus $T^{-1/2}$ for the $SmNiO_3$ film to verify Efros-Shklovskii VRH (ES-VRH) transport mechanism (d) ρ versus T characteristics plotted as $\ln(\rho)$ versus $T^{-1/4}$ for the $SmNiO_3$ film to verify Mott VRH transport mechanism. (e) Magnetization M and the numerical derivative dM/dT of a 25 nm $SmNiO_3$ thin film measured as a function of temperature in μ_o H = 0.1 T. The minimum in dM/dT at approximately 230 ± 20 K indicates the approximate anti-ferromagnetic transition temperature.

(Fig. 2(b)); $\alpha = -1/2$ indicates Efros-Shklovskii variable range hopping (ES-VRH) (Fig. 2(c)); and $\alpha = -1/4$ is characteristic of Mott VRH (Fig. 2(d)). The data in Figs. 2(b)–2(d) indicate that the transport is dominated by the VRH processes (Figs. 2(c) and 2(d)), both of which exhibit a much better linear piece-wise fit ($R^2 > 99.5\%$) than the Arrhenius-type conductivity (Fig. 2(b)). It is also evident that there are two distinct regimes in each VRH process (Figs. 2(c) and 2(d)) with inflection points between the two regimes corresponding to $T \sim 250$ K and $T \sim 280$ K for the ES-VRH (Fig. 2(c)) and Mott-VRH (Fig. 2(d)) models, respectively. This inflection point could be a result of a paramagnetic to the anti-ferromagnetic phase transition in $SmNiO_3$.[20] To confirm this, the magnetization of a 25 nm thick $SmNiO_3$ sample was measured in a SQUID magnetometer (Quantum Design) during field-cooling from 325 K in an external magnetic field of μ_o H = 0.1 T. A blank $LaAlO_3$ substrate was measured separately under identical conditions and its contribution was subtracted to obtain the net signal from the film. The magnetization M as a function of temperature is shown in Fig. 2(e). In order to determine T_N, the numerical derivative of M(T) was calculated (Fig. 2(e)), and T_N was estimated from the minimum of the signal to be 230 K ± 20 K. The weak AF signal and the value of T_N determined in this way was consistent with previous measurements on $SmNiO_3$ bulk ceramic samples.[16,17] The proximity of the inflection point ($T \sim 250$ K) (in the ES-VRH case; Fig. 2(c)) to the T_N, within uncertainty, along with the strong correlation effects known to exist in this material system suggests that the transport mechanism is dominated by ES-VRH. The two distinct regimes in the ES-VRH process separated by the inflection point (closely corresponding to T_N) imply that even though the transport process across this transition may not change fundamentally, the lattice distortions related to the magnetic transition could modify the ES-VRH (temperature independent) transport parameters. In the ES-VRH transport regime, $\rho \propto \exp\left(\frac{T_{ES}}{T}\right)^{1/2}$, where T_{ES} is the characteristic Efros-Shklovskii temperature. The corresponding fits to the data shown in Fig. 2(c) yielded the following T_{ES} values: $T_{ES,1} = 1.62 \times 10^4$ K ($0.0594\ K^{-1/2} < T^{-1/2} < 0.12\ K^{-1/2}$) and $T_{ES,2} = 2.65 \times 10^4$ K ($0.0522\ K^{-1/2} < T^{-1/2} < 0.0594\ K^{-1/2}$).

Next, we studied the electrically (DC) driven phase transition in $SmNiO_3$ (Fig. 3(a)) at different temperatures. Well below the IMT ($T = 273$ K, 333 K in Fig. 3(a)), the current-electric field characteristics were linear at low fields indicative of the insulating state of $SmNiO_3$. The current then became non-linear (more pronounced at lower temperature $T = 273$ K) at higher fields, indicating the initiation of the IMT in $SmNiO_3$. In the metallic state ($T = 403$ K), the current was linear until at high electric field, additional Joule heating resulted in increased resistance and therefore reduced current. To study

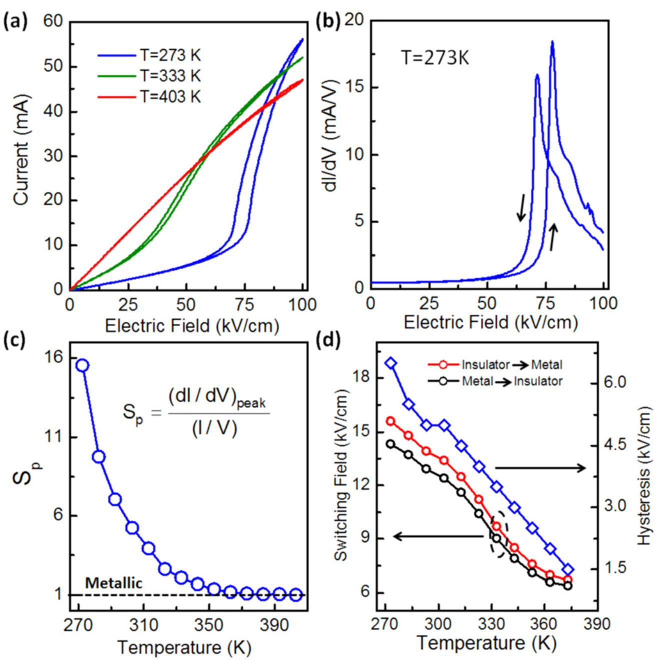

FIG. 3. (a) DC versus applied electric field characteristics for the $SmNiO_3$ thin film at 273 K, 333 K, and 403 K (*I-V* characteristics have been studied between 273 K and 403 K; only three temperatures are shown here). (b) Differential conductance dI/dV as a function of applied electric field at 273 K. (c) S_p as a function of applied electric field. Reduced S_p at higher temperature indicates a smaller change in conductance across the phase transition. (d) Switching fields (corresponding to peak dI/dV value) associated with insulator to metal and metal to insulator transition and hysteresis as a function of temperature. Hysteresis is defined as the difference (in electric field) at which the dI/dV peaks occur during the forward and reverse sweep.

the evolution of the $SmNiO_3$ film resistance/conductance across the electrically driven IMT, we analyzed the differential conductance dI/dV (only $T = 273$ K shown here) as a function of the applied electric field (voltage) (Fig. 3(b)). As the voltage was increased, dI/dV increased (beyond the linear regime), until it peaked at ∼80 kV/cm. This peak corresponds to the field (switching field) at which the non-linearity introduced by the IMT is the largest. A further increase of the electric field resulted in a decrease of dI/dV until it nearly reached a constant value (not shown) implying that the evolution to the metallic state was complete. Further, the switching field was reduced at higher temperature as we approached T_{IMT} (Fig. 3(d)). This gradual rise and decay of dI/dV over a finite electric field (voltage) range implies that the evolution from the insulating to the metallic state is not abrupt, in contrast to some other IMT materials like VO_2 (Ref. 21) and V_2O_3 (Ref. 22) that exhibit an abrupt transition.

The evolution of the electrically driven IMT in $SmNiO_3$ was investigated by calculating the peak value of dI/dV as a function of temperature (Fig. 3(c)). The $(dI/dV)_{peak}$ value was normalized to the conductance I/V since the peak appears at different current and voltage values at different temperatures, so that $S_p = \left(\frac{dI}{dV}\right)_{peak} / \left(\frac{I}{V}\right) = \left(\frac{dI/I}{dV/V}\right)$ (Fig. 3(c)). S_p quantifies the electrically driven change in resistivity across the IMT. From Fig. 3(c), it is clear that S_p decreased as the measurement temperature approached T_{IMT}. This was expected since the resistivity of the film at higher temperature was closer to the metallic state resistivity, and hence, the change in resistance (indicated by dI/dV) required to turn the film metallic is smaller.

The hysteresis in the electrically induced IMT as a function of temperature (Fig. 3(d)) was reduced as T approached T_{IMT}. To explain this observation, we assume that the IMT in $SmNiO_3$ is electro-thermally triggered. The electro-thermal nature of the IMT in $SmNiO_3$ will be confirmed in the following sections. The sample was initially at a temperature T (= ambient temperature). As the voltage was increased, joule heating due to the current flow increased the local temperature of the sample. Hence, the sample temperature in the metallic low resistance state was much higher than T. As the field was swept back, $SmNiO_3$ was at an elevated temperature, and hence, the effective "turn off" voltage to return to the insulating state was lower. The hysteresis is therefore proportional to $\Delta = T_{ON} - T$, where T_{ON} is the temperature of the $SmNiO_3$ film in the metallic state. For $T \rightarrow T_{IMT}$, Δ is smaller, and hence, the hysteresis observed was also less pronounced. While the above observations strongly point to a current induced joule heating driven IMT in $SmNiO_3$, these alone may not be sufficient to qualify Joule heating as the fundamental mechanism driving the IMT (other mechanisms like field induced resistance switching proposed by Sugimoto *et al.*[23] may have similar hysteresis characteristics).

To confirm whether the IMT was electro-thermally triggered, pulsed *I-V* measurements were performed to analyze the IMT response to electrical stimuli applied on a wide time scale (200 ns–10 s). Figure 4(a) shows the circuit schematic for the pulsed *I-V* measurements consisting of a two-terminal $SmNiO_3$ device with a 50 Ω series resistor (R_s; input impedance of oscilloscope). Triangular ramp pulses (Fig. 4(a)) with a peak amplitude of 20 V and time period (τ) ranging from 200 ns to 10 s were applied.[24] The output voltage (V_{Rs}) was measured across R_s. Figure 4(b) shows V_{Rs} for $\tau = 10$ s, 5 ms, 700 μs, and 1 μs (all the outputs are not shown for brevity) at $T = 298$ K. Similar measurements were also performed at $T = 323$ K and 348 K. Two features are clearly evident in the output characteristics: (a) the inflection corresponding to the change in resistance triggered by the IMT decreases with decreasing pulse period. This implies that the IMT was incomplete for shorter pulses; and (b) the peak output voltage V_{peak} (across R_S) reduced with decreasing pulse width indicating that the $SmNiO_3$ film progressively undergoes a smaller change in conductance for shorter pulses (Fig. 4(c)). The absence of non-linearity in the $\tau = 1\,\mu$s pulse implied the absence of an IMT (Fig. 4(b)). The critical pulse times τ_{cr} below which no non-linearity was observed are $\tau_{cr} = 100\,\mu$s ($T = 298$ K);=50 μs ($T = 323$ K); = 1 μs ($T = 348$ K).

The strong sensitivity of the non-linear change in resistance (induced by the IMT) to the time period of the applied pulse confirms that the phase transition in $SmNiO_3$ is driven by current induced self-heating.[25–28] Figure 4(d) shows the energy supplied through the input pulse and non-linear change in resistivity (resulting from the IMT) quantified as dI/dV as a function of τ. It is evident that the dI/dV (indicating change in resistance) decreased with shorter pulse periods and then became constant implying no IMT. This is because the input energy (to be converted to Joule heat) was reduced, causing insufficient self-heating to initiate the IMT. Further, it is important to note that the peak electric field across the device (corresponding to $V_{in} = 20$ V) remained nearly constant. Therefore, the possibility of the

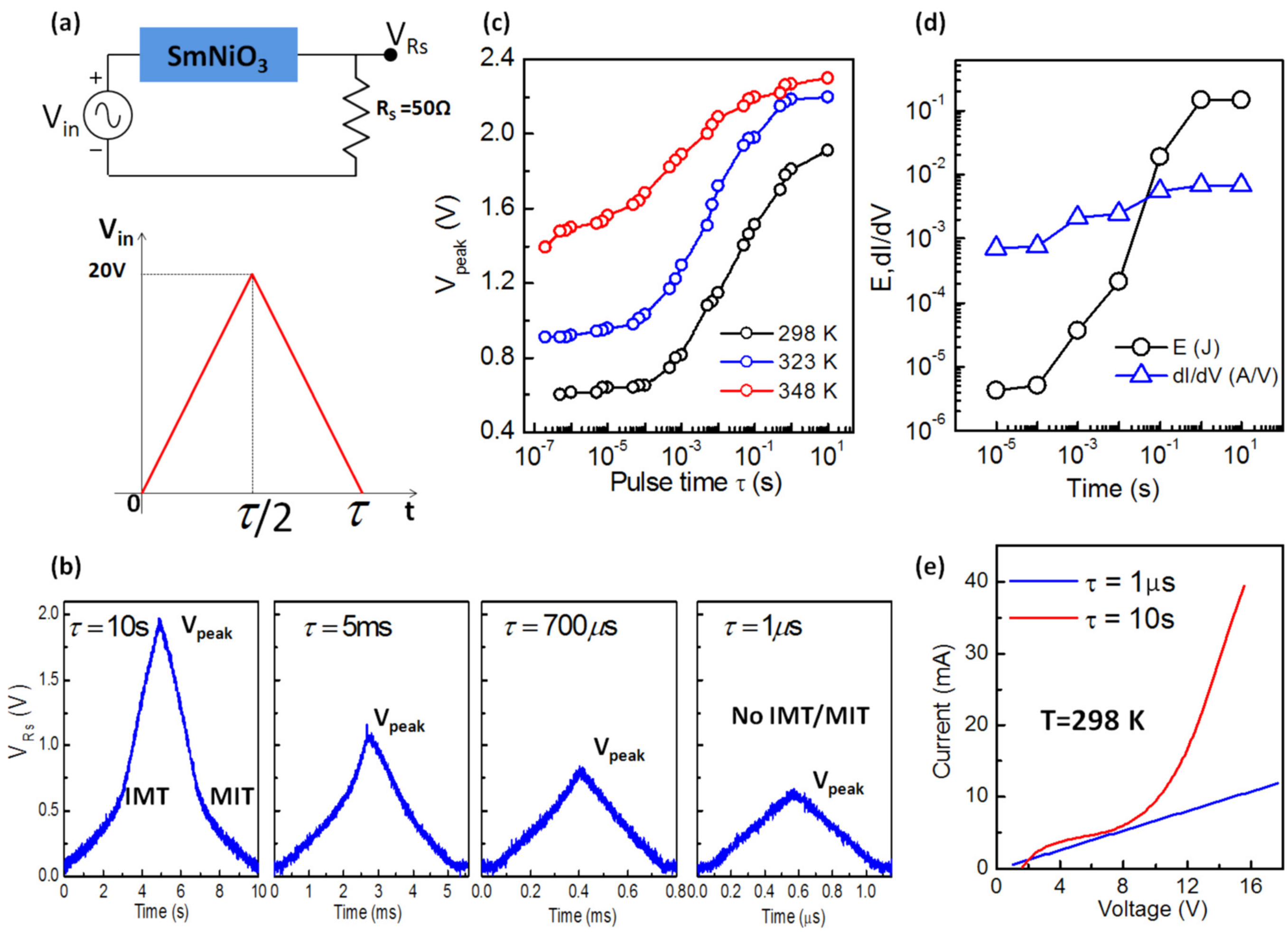

FIG. 4. (a) Schematic of the circuit and the input voltage ramp pulse used for pulsed mode current-voltage measurements. The output voltage is measured across a 50 Ω resistance (R_s). The amplitude of the voltage pulse is 20 V, while τ ranges from 200 ns to 10 s. (b) Output voltage for different time periods $\tau = 10$ s, 5 ms, 700 μs and 1 μs. The non-linearity and the peak output voltage decreases progressively as τ is reduced. (c) Variation of peak output voltage V_{peak} as a function of input time period τ of the pulse for different temperatures. (d) Input energy and dI/dV (indicating change in resistance due to IMT) as a function of input time period τ of the pulse ($T = 298$ K). Similar trends are observed at 323 K and 348 K. Here, energy refers to input energy supplied to $SmNiO_3$ film (in the insulating state) until IMT occurs. (e) Current versus voltage characteristics across the $SmNiO_3$ device for different pulse time periods. $\tau = 10$ s shows a non-linear change in resistance indicating IMT. For the $\tau = 1$ μs pulse, the resistance is constant implying that no IMT occurs.

IMT in $SmNiO_3$ being driven by a purely electric field effect[23] is unlikely.

From the I-V characteristics (across the $SmNiO_3$ device), for the $\tau = 10$ s and $\tau = 1$ μs case (Fig. 4(e)), it is evident that the *I-V* characteristics for the 1 μs pulse were linear, indicating that the resistance was constant and no IMT was triggered despite of the peak input ramp voltage (=20 V) remaining the same. Unlike the $\tau = 1$ μs case, the $\tau = 10$ s case had a non-linear evolution of the resistance, indicative of the occurrence of an IMT.

We now discuss our results in the context of the nature of the IMT in $SmNiO_3$. The rare earth nickelates $RNiO_3$ are classified as charge transfer insulators according to the Zaanen-Sawatzky-Allen criteria[29] for correlated oxides, with the insulating band-gap formed between the oxygen 2p and the Ni 3d bands. In case of the nickelates, the overlap of the lower Hubbard band with the oxygen p band depends on the angles of the Ni-O bonds. This so-called negative or zero charge transfer[30] causes a strong dependence of the band gap on the Ni^{3+}-O^{2-} hybridization and its geometrical arrangement.

Recent studies[31–33] have pointed out the importance of a two Ni-site distribution, between the more ionic Ni1 and the more covalent Ni2 sites with longer and shorter Ni-O bonds, respectively, which are present in the low temperature insulating phase, described within the monoclinic $P2_1/n$ space group. Johnston *et al.*[34] recently proposed that the IMT in nickelates originates from a strong coupling between the O ligand holes as charge carriers and the rocksalt-like lattice distortions related to the Ni1 and the Ni2 sites in distinct $(NiO_6)^{3-}$ octahedra.

When $SmNiO_3$ is electrically driven, Joule self-heating results in a reduction of the lattice distortion in the insulating phase and in the corresponding band gap closure.[34] The transport properties in the metallic state remain affected by the electron-phonon interactions. This was corroborated by Jaramillo *et al.*[12] who observed that a mid-infrared peak corresponding to the bandgap-like feature in the insulating state persists as a Holstein polaronic side band in the metallic state. Mediated via electron-lattice interaction, gradual band structure transformation with increasing temperature results in a non-linear increase in the conductivity as observed experimentally. Further, with pulse I-V measurements, the increase in local temperature induced by Joule heating becomes progressively smaller, and therefore the non-linear increase in resistivity induced by the IMT diminishes.

In summary, we have investigated the IMT in epitaxial $SmNiO_3$ thin films grown on (001) $LaAlO_3$. Temperature dependent resistivity measurements indicate that Efros-Shkloskii VRH is likely to be the dominant transport mechanism in the insulating state of $SmNiO_3$. Further, we explore the electrically driven IMT in $SmNiO_3$ through DC and pulse I-V measurements over a large time scale elucidating the fundamental mechanism driving the IMT in $SmNiO_3$ to be current induced Joule self-heating.

The authors thank Professor Roman Engel-Herbert, Dr. Steve Kramer, and Himanshu Madan for fruitful discussions. Some of the authors at PSU acknowledge support from the Office of Naval Research through Award No. N00014-11-1-0665. Work at PSU and WVU was supported by STARnet, a Semiconductor Research Corporation program, sponsored by MARCO and DARPA. Additional support for the work at WVU came from a Higher Education Policy Commission Research Challenge Grant and the WVU Shared Research Facilities.

[1]M. Imada, A. Fujimori, and Y. Tokura, Rev. Mod. Phys. **70**, 1039 (1998).
[2]P. D. C. King, H. I. Wei, Y. F. Nie, M. Uchida, C. Adamo, S. Zhu, X. He, I. Božović, D. G. Schlom, and K. M. Shen, Nat. Nanotechnol. **9**, 443 (2014).
[3]J. Chaloupka and G. Khaliullin, Phys. Rev. Lett. **100**, 016404 (2008).
[4]R. Scherwitzl, P. Zubko, C. Lichtensteiger, and J.-M. Triscone, Appl. Phys. Lett. **95**, 222114 (2009).
[5]H. Huang, Z. Luo, Y. Yang, Y. Yun, M. Yang, D. Meng, H. Wang, S. Hu, J. Bao, Y. Lu, and C. Gao, AIP Adv. **4**, 057102 (2014).
[6]R. Scherwitzl, S. Gariglio, M. Gabay, P. Zubko, M. Gibert, and J.-M. Triscone, Phys. Rev. Lett. **106**, 246403 (2011).
[7]R. Scherwitzl, P. Zubko, I. G. Lezama, S. Ono, A. F. Morpurgo, G. Catalan, and J.-M. Triscone, Adv. Mater. **22**, 5517 (2010).
[8]R. Scherwitzl, "Metal-insulator transitions in nickelate heterostructures," Ph.D. thesis (University of Geneva, 2012).
[9]J. Son, P. Moetakef, J. M. LeBeau, D. Ouellette, L. Balents, S. J. Allen, and S. Stemmer, Appl. Phys. Lett. **96**, 062114 (2010).
[10]J. Son, B. Jalan, A. P. Kajdos, L. Balents, S. James Allen, and S. Stemmer, Appl. Phys. Lett. **99**, 192107 (2011).
[11]J. Son, J. M. LeBeau, S. J. Allen, and S. Stemmer, Appl. Phys. Lett. **97**, 202109 (2010).
[12]R. Jaramillo, S. D. Ha, D. M. Silevitch, and S. Ramanathan, Nat. Phys. **10**, 304 (2014).
[13]J. S. Zhou, J. Goodenough, and B. Dabrowski, Phys. Rev. Lett. **95**, 127204 (2005).
[14]G. Catalan, Phase Transitions **81**, 729 (2008).
[15]J. B. Torrance, P. Lacorre, A. I. Nazzal, E. J. Ansaldo, and C. Niedermayer, Phys. Rev. B **45**, 8209 (1992).
[16]J. Pérez, J. Blasco, J. García, M. Castro, J. Stankiewicz, M. C. Sánchez, and R. D. Sánchez, J. Magn. Magn. Mater. **196–197**, 541 (1999).
[17]J. Pérez-Cacho, J. Blasco, J. García, M. Castro, and J. Stankiewicz, J. Phys. Condens. Matter **11**, 405 (1999).
[18]S. Ha, B. Viswanath, and S. Ramanathan, J. Appl. Phys. **111**, 124501 (2012).
[19]J. Shi, S. D. Ha, Y. Zhou, F. Schoofs, and S. Ramanathan, Nat. Commun. **4**, 2676 (2013).
[20]S. Ha, R. Jaramillo, D. Silevitch, F. Schoofs, K. Kerman, J. Baniecki, and S. Ramanathan, Phys. Rev. B **87**, 125150 (2013).
[21]H.-T. Kim, B.-G. Chae, D.-H. Youn, S.-L. Maeng, G. Kim, K.-Y. Kang, and Y.-S. Lim, New J. Phys. **6**, 52 (2004).
[22]J. Brockman, "Electric field-induced conductivity switching in vanadium sesquioxide nanostructures," Ph.D. thesis (Stanford University, 2012).
[23]N. Sugimoto, S. Onoda, and N. Nagaosa, Phys. Rev. B **78**, 155104 (2008).
[24]The following time periods were used. $\tau = 200$ ns, 500 ns, 700 ns, 1 μs, 5 μs, 7 μs, 10 μs, 50 μs, 70 μs, 100 μs, 500 μs, 700 μs, 1 ms, 5 ms, 7 ms, 10 ms, 50 ms, 100 ms, 500 ms, 700 ms, 1 s, 10 s.
[25]B. Fisher, J. Genossar, L. Patlagan, and G. M. Reisner, EPJ Web Conf. **40**, 15009 (2013).
[26]B. Fisher, J. Genossar, K. B. Chashka, L. Patlagan, and G. M. Reisner, Acta Phys. Pol. A **111**, 57 (2007).
[27]B. Fisher, J. Genossar, K. B. Chashka, L. Patlagan, and G. M. Reisner, Appl. Phys. Lett. **104**, 153511 (2014).
[28]B. Fisher, J. Genossar, L. Patlagan, and G. M. Reisner, J. Magn. Magn. Mater. **322**, 1239 (2010).
[29]J. Zaanen, G. Sawatzky, and J. Allen, Phys. Rev. Lett. **55**, 418 (1985).
[30]T. Mizokawa, A. Fujimori, T. Arima, Y. Tokura, N. Mori, and J. Akimitsu, Phys. Rev. B: Condens. Matter **52**, 13865 (1995).
[31]H. Park, A. J. Millis, and C. A. Marianetti, Phys. Rev. Lett. **109**, 156402 (2012).
[32]B. Lau and A. Millis, Phys. Rev. Lett. **110**, 126404 (2013).
[33]J. A. Alonso, M. J. Martínez-Lope, I. A. Presniakov, A. V. Sobolev, V. S. Rusakov, A. M. Gapochka, G. Demazeau, and M. T. Fernández-Díaz, Phys. Rev. B **87**, 184111 (2013).
[34]S. Johnston, A. Mukherjee, I. Elfimov, M. Berciu, and G. A. Sawatzky, Phys. Rev. Lett. **112**, 106404 (2014).